PCCP

Cite this: *Phys. Chem. Chem. Phys.*, 2011, **13**, 16146–16149

www.rsc.org/pccp

COMMUNICATION

Insights into the structure of the active site of the O_2-tolerant membrane bound [NiFe] hydrogenase of *R. eutropha* H16 by molecular modelling†

Yvonne Rippers,‡ Tillmann Utesch,‡ Peter Hildebrandt, Ingo Zebger and Maria Andrea Mroginski

Received 4th April 2011, Accepted 27th July 2011
DOI: 10.1039/c1cp21045a

Structural models for the Ni-B state of the wild-type and C81S protein variant of the membrane-bound [NiFe] hydrogenase from *Ralstonia eutropha* H16 were derived by applying the homology model technique combined with molecular simulations and a hybrid quantum mechanical/molecular mechanical approach. The active site structure was assessed by comparing calculated and experimental IR spectra, confirming the view that the active site structure is very similar to those of anaerobic standard hydrogenases. In addition, the data suggest the presence of a water molecule in the second coordination sphere of the active centre.

Hydrogenases are enzymes which catalyse the reversible heterolytic cleavage of molecular hydrogen. In the focus of our study are [NiFe] hydrogenases, in which the catalytic site is a bimetallic complex, with two Ni bound terminal cysteine residues, three exogenous diatomic inorganic ligands (one CO and two CN^-) at the Fe atom, and two further cysteines bridging the two metal atoms.[1] Depending on the particular redox state another, different ligand may occupy an additional bridging position between Ni and Fe. Most members of this enzyme family are oxygen-sensitive and form under electron-deficient conditions with O_2 the so-called 'unready inactive' Ni_u-A state, that requires a rather long time (up to several hours) for a reductive (re-)activation by molecular hydrogen, a property that impairs practical applications.[1] The membrane-bound [NiFe] hydrogenase (MBH) from *Ralstonia eutropha* H16 (*Re*H16), however, is capable of oxidizing hydrogen even at atmospheric oxygen levels. Under these conditions only the so-called 'ready inactive' Ni_r-B state is formed which is rapidly reactivated on the (sub-)second time scale, while the Ni_u-A state has never been observed for the wild type MBH.[2,3] Therefore, this enzyme appears to be a promising candidate in the field of biotechnological energy storage and conversion as an alternative to fossil fuels.[4] Ni_r-B harbors a hydroxide in the bridging position between Ni and Fe,[5,6] while a hydroperoxide is suggested to be the bridging ligand in Ni_u-A.[7] These two states can be distinguished by IR spectroscopy which, in general, is a particularly instructive method for the identification of the various redox states involved in the catalytic cycle by probing the stretching modes of the CO and CN^- ligands.[8,9]

So far, however, no crystallographic structures of oxygen tolerant [NiFe] hydrogenases have been reported, which would facilitate a more detailed investigation of the underlying reaction mechanism at the active site. In this work, we have constructed a homology model for the MBH from *Re*H16 using the known three-dimensional (3D) structures of the standard [NiFe] hydrogenases as a template. The homology model was further refined by molecular dynamics (MD) simulations and quantum-mechanics/molecular mechanics (QM/MM) geometry optimizations of the active site, followed by the calculation of the IR spectra. Three structural models of the oxidized MBH in the Ni_r-B state were generated: MBH wild type (*MBH* model), MBH wild type including a water molecule in the second coordination sphere of the [NiFe] center as detected in other 3D structures of oxygen-sensitive hydrogenases (*MBH-H_2O* model) and the C81S variant MBH (*MBH-C81S-H_2O* model) which also contains the extra water. The latter protein variant was chosen because the mutation induces a significant 8 cm^{-1} shift of the CO stretching in the experimental IR spectrum.[10] Hence, the reproduction of a mutation-induced shift is considered as a more reliable criterion for the quality of the homology model in the active site than a comparison between the wild type MBH and the template enzyme *D. gigas* for which the frequency difference was only 2 cm^{-1} and thus close to the experimental accuracy. The quality of the resulting structures was further evaluated *via* a Ramachandran plot analysis[11] (see Fig. S2 in the ESI†).

The far-reaching sequence identity between the template and the target of 44% leads to an initial model structure with a low overall root-mean-square deviation (with respect to the template) of 0.8 Å for the backbone atoms of both the small and the large subunit. This is particularly true for the environment of the bimetallic center, constituted by highly conserved amino acids. As a consequence, the active structure in the homology model is essentially the same as for the template. In this region only minor structural differences were observed due

Institut f. Chemie, Sekr. PC14, Technische Universität Berlin, Straße des 17, Juni 135, D-10623 Berlin, Germany. E-mail: andrea.mroginski@tu-berlin.de; Fax: +49 30 31421122; Tel: +49 30 31426403

† Electronic supplementary information (ESI) available. See DOI: 10.1039/c1cp21045a

‡ These authors contributed equally to the work and are listed alphabetically.

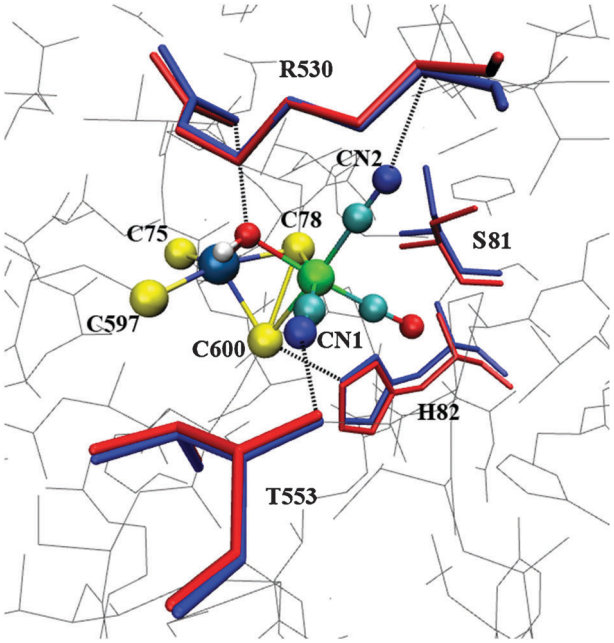

Fig. 1 Active site structure of *MBH-C81S* including a water molecule in the second coordination sphere (not displayed for the sake of clarity) and the amino acids R530, T553, H82 and S81 in two conformations (blue and red). Dashed lines indicate hydrogen bonds. The atoms of the bimetallic centre are represented by balls (S, yellow; O, red; C, cyan; N, blue; H, white; Ni, dark blue; Fe, green). Grey lines represent the protein matrix; all amino acids are shown without hydrogen atoms.

to the replacement of threonine by a serine at position 553. Larger deviations in the homology models are noted in surface loop regions. In all three structural models, important secondary structure elements are conserved (see Fig. S3 in the ESI†).

As observed in standard hydrogenases, the active sites in all our calculated models are embedded in the protein forming coordinative bonds between the metals and cysteine residues. Furthermore, the bimetallic centre is stabilized by a hydrogen bond network including, among others, interactions between the cyanide ligands CN and CN2 to the backbone nitrogens of T553 and R530, respectively. Except for the *MBH* model stable hydrogen bonds are established between the OH^- bridge and the side-chain nitrogen of R530. For all models only weaker hydrogen bonds are formed between the bridging sulfur of C78 or C600, respectively, and the N_ε of H82 located in the first coordination sphere, as described previously[12] (Fig. 1). It is interesting to note that the analysis of the MD trajectories for the *MBH-C81S-H_2O* model reveals two distinct conformations associated with Ser81 (Fig. 1).

The active site optimized by QM/MM calculations is a very rigid construct reflected by very low standard deviations computed over the series of snapshots (see Table S3 in the ESI†). A comparison with the crystallographic structure of *D. gigas* (2FRV),[13] also harboring two CN^- and one CO ligands, indicates a shortening of the Fe–OH^-, the Ni–S(C78), the Ni–S(C597) and the Ni–S(C600) bonds in the optimized structure. The length of the Fe–CO bond is reduced from 1.87 Å in the crystallographic structure to around 1.72 Å in our model. The Fe–CN1 bond is very similar in length to the crystallographic structure, while the Fe–CN2 bond is elongated to 1.90 Å in our model (2FRV: 1.67 Å). This comparison further supports the view of a standard hydrogenase-like catalytic centre in the MBH. Compared to previous theoretical calculations performed on the active site of *D. gigas* in the Ni-B state,[14] the differences in the crystallographic structures are reduced in the present model except for a slightly larger difference for the Ni–S(C533) and Ni–OH^- bonds. Earlier theoretical models presented by Stein and Lubitz[15] display even higher differences, which might be related to the exclusion of the protein charge cloud (see Table S5 in the ESI†).

To validate the derived structural model of the catalytic centre IR spectra of the [NiFe] centre were computed (see Methods) and compared with the corresponding experimental data.[10] A similar procedure has been employed in the past for determining the structure of a guanosine triphosphate (GTP) ligand bound to a Ras protein.[16] Calculated spectra were obtained from 25 snapshots of the MD trajectory. The average frequencies and their standard deviations are listed in Table 1. The experimental IR spectrum in the region between 1890–2110 cm^{-1} exclusively displays the stretching modes of the inorganic ligands with a prominent band at 1947 cm^{-1} originating from the CO stretching vibration, and two weaker bands at 2080 cm^{-1} and 2098 cm^{-1} assigned to the asymmetric and symmetric CN stretching modes, respectively.[2] In the IR spectrum of the C81S MBH mutant, the CO stretching mode is shifted to higher wavenumbers by 8 cm^{-1} whereas the CN stretching modes remain largely unchanged.[10]

In the *MBH* model consisting of a QM partition of 26 atoms (*vide infra*), analysis of the calculated spectra shows an overestimation of the vibrational frequencies of the CO and CN stretching modes, ν(CO) and ν(CN), compared to the experimental values (Table 1). Incorporation of water adjacent to the [NiFe] centre significantly improves the estimated ν(CO) frequency, which is now predicted at 1950 cm^{-1} and thus very close to the experimental value. However, the frequencies of the CN stretching modes are still overestimated. In presence of water, C81 is forced towards the CO ligand such that the CO–HS distance decreases from 6.4 Å in the *MBH* model to only 2.4 Å in the *MBH-H_2O* model. A further improvement is achieved by enlarging the QM partition to 75 atoms, including R530, T553, and H82 which are involved in hydrogen bond interactions with the CN ligands and the OH bridging ligand. With this model, not only the CO stretching is very well reproduced but also the CN stretching modes are predicted at much lower frequencies such that they coincide distinguished with the experimental values. The difference between

Table 1 Calculated and experimental frequencies (in cm^{-1}) for the wild type MBH and the C81S mutant. The calculated average frequencies are accompanied by the standard deviations computed over 25 spectra

		ν(CO)	$\nu(CN)_{asym}$	$\nu(CN)_{sym}$
Exp.	MBH-WT	1947	2080	2098
Calc.	MBH (QM26)	1970 ± 4	2106 ± 4	2120 ± 4
	MBH-H_2O (QM26)	1950 ± 5	2097 ± 6	2128 ± 5
	MBH-H_2O (QM75)	1954 ± 5	2078 ± 4	2098 ± 3
Exp.	MBH-C81S	1955	2080	2097
Calc.	MBH-C81S-H_2O (QM75)	1959 ± 8	2081 ± 12	2110 ± 5

the ν(CN) frequencies computed for the *MBH* and *MBH-H_2O* models appear to be related to minor structural changes of the environment, such as the twisting of the R530 and the T553 side chains.

Also the IR spectra calculated for the *MBH-C81S-H_2O* model exhibit a very good agreement with the experimental IR spectrum. The experimental frequency upshift of 8 cm^{-1} compared to the WT protein is very well reproduced by the calculations. The good agreement also holds for the asymmetric CN stretching while only the symmetric CN stretching is overestimated by the calculations. The frequency upshift of the CO stretching can be explained as a consequence of the higher polarity of the serine side chain, which is represented by a larger negative point charge, reducing the backbonding from the iron and strengthening the CO bond (blue-shifted).[8] On the other hand, the CO stretching frequency calculated for the *MBH-C81S-H_2O* model is lower by 10 cm^{-1} compared to that of the *MBH* model lacking the internal water molecule. Thus, the comparison of the experimental and calculated spectra for the WT and C81S variants provides strong support for a water molecule close to the [NiFe] centre. Note that the variations of the CN stretching frequencies for the *MBH-C81S-H_2O* model are larger than for the WT model, which is attributed to the fluctuations of the hydrogen bond network involving the CN^- ligands.

For the *MBH-H_2O* model and the *MBH-C81S-H_2O* model, calculated potential energy distributions show that the asymmetric ν(CN) mode is dominated by the stretching of the CN1 ligand, while the symmetric ν(CN) mode mainly contains the stretching of the CN2 ligand. Interestingly, there is a change of the hydrogen bond network involving H82 and the bridging cysteines. For the WT MBH, the hydrogen bond is formed with the sulfur atom of C78 whereas for the C81S mutant, it is formed with the bridging sulfur atom from C600. Analysis of the 25 snapshot structures with their corresponding vibrational spectra shows that there is a linear correlation between the strength of this hydrogen bond and the ν(CO) frequency: a stronger hydrogen bond is reflected by an increase of the ν(CO) frequency.

In summary, the theoretical 3D structural models of the MBH show only minor structural rearrangements of the active site and its vicinity compared to standard hydrogenases. These results confirm previous suggestions[2,3,24] of a very similar catalytic centre in oxygen-tolerant and -sensitive [NiFe] hydrogenases, ruling out that the molecular origin of the oxygen-tolerance of MBH is related to a specific modification at the catalytic centre. The reliability of the present structural model for the active site of MBH, with a high similarity to oxygen-sensitive "standard" [NiFe] hydrogenases, is supported by the distinguished agreement between experimental and the QM/MM calculated IR spectra and specifically by the reproduction of the IR spectroscopic changes related to a single mutation of C81 to serine located in the second coordination sphere of the active site. In addition, these calculations indicate a water molecule close to C81, which influences the IR spectra. The present results constitute another example[16] where the combination of molecular modelling with a spectroscopic validation represents a valuable tool for the structural analysis of enzymes for which no crystal structures are available.

Methods

Homology modeling

The MBH homology models were constructed with Modeller v9.5[17] using the structures of the standard hydrogenases of *inter alia D. vulgaris* Miyazaki F[18] and *D. gigas*[13] as a template for the overall protein and the active site structure, respectively. Based on spectroscopic studies, the structure of the Ni-B state of the active site includes one CO, and two CN^- ligands and an OH^- bridging ligand.[5,6] In the *MBH-H_2O* model, one water molecule was added adjacent to the active site. The C81S variant structure was constructed by replacing C81 by a serine followed by a short energy minimization run. Following the same procedure as for the *MBH-H_2O* model, a water molecule was placed in the active site cavity of the C81S mutant. MD simulations were performed to relax and to equilibrate the three structural models in TIP3P water boxes.[19] The internal motions of the [NiFe] centre and the Fe–S clusters were strongly constrained during the MD simulations (see ESI 1†).

Geometry optimization of the active site

25 snapshots were extracted from the MD trajectory. The respective geometries were optimized at the QM/MM level of theory by combining density functional theory (DFT) calculations using the BP86 functional with CHARMM22 force field. The QM part consists either of 26 atoms containing the bimetallic centre with Ni(III) and Fe(II), the exogenous ligands, and the side chains of the four coordinating cysteines, or of 75 atoms by including R530, T553, and H82. The 6-31g(d) basis set was applied for all atoms excluding Ni and Fe for which Ahlrichs triple-zeta polarization all electron basis set (TZVP) was employed.[20] Covalent bonds at the QM/MM border were cut and saturated by hydrogen link atoms. The coupling between QM and MM was computed using electrostatic embedding with a charge-shift scheme.[21] Final models were constructed by averaging over the 25 individual structures (see ESI 4†).

Spectra calculation

IR spectra of the active site were calculated for each snapshot using the normal mode analysis approximation following the procedure described previously by Mroginski *et al.*[22] The final IR spectra for each model were computed using the instantaneous normal mode analysis (INMA) approach.[23]

Acknowledgements

We thank the DFG (Cluster of Excellence "UniCat") for financial support and the "Norddeutscher Verbund für Hoch- und Höchstleistungsrechnen" (HLRN) for providing computer resources.

Notes and references

1 J. C. Fontecilla-Camps, A. Volbeda, C. Cavazza and Y. Nicolet, *Chem. Rev.*, 2007, **107**, 4273–4303.
2 M. Saggu, I. Zebger, M. Ludwig, O. Lenz, B. Friedrich, P. Hildebrandt and F. Lendzian, *J. Biol. Chem.*, 2009, **284**, 16264–16276.
3 O. Lenz, M. Ludwig, T. Schubert, I. Bürstel, S. Ganskow, T. Goris, A. Schwarze and B. Friedrich, *ChemPhysChem*, 2010, **11**, 1107–1119.

4 K. A. Vincent, J. A. Cracknell, O. Lenz, I. Zebger, B. Friedrich and F. A. Armstrong, *Proc. Natl. Acad. Sci. U. S. A.*, 2005, **102**, 16951–16954.
5 A. J. Pierik, W. Roseboom, R. P. Happe, K. A. Bagley and S. P. J. Albracht, *J. Biol. Chem.*, 1999, **274**, 3331–3337.
6 M. van Gastel, M. Stein, M. Brecht, O. Schröder, F. Lendzian, R. Bittl, H. Ogata, Y. Higuchi and W. Lubitz, *J. Biol. Inorg. Chem.*, 2006, **11**, 41–51.
7 A. Volbeda, L. Martin, C. Cavazza, M. Matho, B. W. Faber, W. Roseboom, S. P. Albracht, E. Garcin, M. Rousset and J. C. Fontecilla-Camps, *J. Biol. Inorg. Chem.*, 2005, **10**, 239–249.
8 A. L. De Lacey, V. M. Fernandez, M. Rousset and R. Cammack, *Chem. Rev.*, 2007, **107**, 4304–4330.
9 M. E. Pandelia, H. Ogata and W. Lubitz, *ChemPhysChem*, 2010, **11**, 1127–1140.
10 M. Saggu, M. Ludwig, B. Friedrich, P. Hildebrandt, R. Bittl, F. Lendzian, O. Lenz and I. Zebger, *ChemPhysChem*, 2010, **11**, 1215–1224.
11 R. W. W. Hooft, G. Vriend, C. Sander and E. E. Abola, *Nature*, 1996, **381**, 272–272.
12 C. Stadler, A. L. de Lacey, Y. Montet, A. Volbeda, J. C. Fontecilla-Camps, J. C. Conesa and V. M. Fernandez, *Inorg. Chem.*, 2002, **41**, 4424–4434.
13 A. Volbeda, E. Garcin, C. Piras, A. L. de Lacey, V. M. Fernandez, E. C. Hatchikian, M. Frey and J. C. Fontecilla-Camps, *J. Am. Chem. Soc.*, 1996, **118**, 12989–12996.
14 P. Jayapal, M. Sundararajan, I. H. Hillier and N. A. Burton, *Phys. Chem. Chem. Phys.*, 2008, **10**, 4249–4257.
15 M. Stein and W. Lubitz, *Phys. Chem. Chem. Phys.*, 2001, **3**, 2668–2675.
16 M. Klähn, J. Schlitter and K. Gerwert, *Biophys. J.*, 2005, **88**, 3829–3844.
17 A. Sali and T. L. Blundell, *J. Mol. Biol.*, 1993, **234**, 779–815.
18 H. Ogata, S. Hirota, A. Nakahara, H. Komori, N. Shibata, T. Kato, K. Kano and Y. Higuchi, *Structure*, 2005, **13**, 1635–1642.
19 W. L. Jorgensen, J. Chandrasekhar, J. D. Madura, R. W. Impey and M. L. Klein, *J. Chem. Phys.*, 1983, **79**, 926–935.
20 F. Weigend and R. Ahlrichs, *Phys. Chem. Chem. Phys.*, 2005, **7**, 3297–3305.
21 D. Bakowies and W. Thiel, *J. Phys. Chem.*, 1996, **100**, 10580–10594.
22 M. A. Mroginski, F. Mark, W. Thiel and P. Hildebrandt, *Biophys. J.*, 2007, **93**, 1885–1894.
23 M. Nonella, G. Mathias and P. Tavan, *J. Phys. Chem. A*, 2003, **107**, 8638–8647.
24 J. Fritsch, S. Löscher, O. Sanganas, E. Sieber, I. Zebger, M. Stein, M. Ludwig, A. L. De Lacey, H. Dau, B. Friedrich and O. Lenz, *Biochemistry*, 2011, **50**, 5858–5869.